J Solid State Electrochem (2018) 22:1449–1458
DOI 10.1007/s10008-017-3771-4

ORIGINAL PAPER

A novel WO_3/MoS_2 photocatalyst applied to the decolorization of the textile dye Reactive Blue 198

Suellen Aparecida Alves[1] · **Lorena Athie Goulart**[1] · **Lúcia Helena Mascaro**[1]

Received: 25 June 2017 / Revised: 4 September 2017 / Accepted: 12 September 2017 / Published online: 17 September 2017

Abstract A novel FTO/WO_3 electrode decorated with MoS_2 was constructed using two simple and low-cost techniques involving a modified single-step sol-gel method for the WO_3 film together with the electrodeposition of amorphous MoS_2. The photoelectrocatalytic performance of the material was investigated by monitoring the degradation of Reactive Blue 198 dye under visible-light irradiation. The FTO/WO_3/MoS_2 electrode exhibited excellent photocatalytic activity and afforded total decolorization of the dye after 90 min at low applied current density (5 mA cm^{-2}). The results described herein support the view that MoS_2 acts as a noble metal-free cocatalyst by promoting H_2 evolution and assisting in the suppression of electron/hole pair recombination in the photocatalytic material (WO_3), thereby improving the process of decolorization of the dye solution. The novel approach of combining of the WO_3 and MoS_2 materials shows particular promise and may prove to be very effective in the photocatalytic degradation of other hazardous organic compounds.

Keywords Photocatalyst · Cocatalysis · Photoelectrochemical degradation · WO_3/MoS_2 electrode · Reactive Blue 198

Electronic supplementary material The online version of this article (https://doi.org/10.1007/s10008-017-3771-4) contains supplementary material, which is available to authorized users.

✉ Lúcia Helena Mascaro
lmascaro@ufscar.br

[1] Universidade Federal de São Carlos, Rodovia Washington Luiz, km 235, São Carlos, São Paolo 13565-905, Brazil

Introduction

The development of novel photocatalysts has focused mainly on the application of semiconductors, but few of these materials afford enhanced photocatalytic efficiency and high stability when illuminated with visible light [1–3]. Thus, the search for new photocatalysts has retained its importance, and investigations continue with the aim of increasing photocatalytic efficiency, most especially by the reduction of spontaneous electron/hole (e^-/h^+) pair recombination.

A number of studies have shown that photoinduced charge separation at the heterointerface of a heterojunction structure is effective in reducing e^-/h^+ recombination [4–10]. Consequently, various heterojunction photocatalysts have been constructed and used in a range of applications, including water splitting and the photocatalytic degradation of organic molecules [11–15]. It is also possible to avoid, at least in part, the recombination of e^-/h^+ by introducing materials such as cobalt–phosphate [16], FeO(OH) [17], IrO_2 [18], and Pt [19] that catalyze O_2 or H_2 evolution reactions. Furthermore, it is possible to add a dopant to a semiconductor to improve the photocatalyst response. Wang et al. synthesized manganese-doped TiO_2 nanoparticles by a near-equilibrium process and they observed photocatalyst properties. The authors evaluated the degradation of organic dye and it was noted a significant improvement in the photodegradation due to manganese presence, especially by low content of oxygen vacancies in the manganese-doped TiO_2 and decrease of particle size [10].

The transition metal oxide WO_3 has been widely employed as a photoanode, but it exhibits a gradual loss of photoactivity during long-term use. It is expected that the formation of a heterojunction catalyst with WO_3 [20, 21], or combination of the semiconductor with a material capable of facilitating charge transfer, would lead to an improvement in photocatalytic performance by preventing e^-/h^+ recombination [22]. In this

context, diverse studies have established that MoS_2 is an interesting material for nanoelectronic applications by virtue of its high electron mobility and considerable stability [23, 24]. The disulfide has been applied in various areas, most especially in energy applications [25–27], and the crystalline form has recently been used in combination with other semiconductor materials to generate heterojunction structures from the staggered band alignment formed between the two structures [28]. Thus, Liu et al. [26] produced TiO_2 nanobelts modified with MoS_2 nanoparticles using a two-step hydrothermal method and showed that the heterojunction structure afforded high photocatalytic activity in the degradation of rhodamine B under visible-light irradiation. A facile hydrothermal method was also employed by Zhao et al. [27] to fabricate a novel p–n heterojunction photocatalyst n-$BiVO_4$/p-MoS_2 with a core–shell structure. This material exhibited excellent photocatalytic activity for the reduction of Cr^{6+} and the oxidation of crystal violet under visible-light irradiation.

The ability of MoS_2 to exert a catalytic effect on H_2 evolution has been exploited by Kibsgaard et al. [28] in the successful application of the material as a cocatalyst. The dichalcogenide can accept an electron photogenerated at a photoanode, resulting in a reduction in e^-/h^+ pair recombination, an increase in anodic photocurrent and, ultimately, enhancement of photocatalytic H_2 production [29]. Moreover, MoS_2 can improve the efficiency of degradation of organic compounds because the electrons can be scavenged by O_2 to yield a superoxide radical anion that can then react to produce $^{\cdot}OH^-$ [30].

An important consideration in the development of new photocatalytic heterojunction structures and composites is the requirement of simple and inexpensive methods of synthesis and material preparation. From a process viewpoint, it is also advantageous if the structures so-formed can be immobilized on the substrate, thereby eliminating the need to remove the photocatalyst from the solution by filtration or centrifugation.

Wastewater from the textile industry constitutes an important source of environmental pollution because of the large volumes involved and the high content of water-soluble contaminants. The azo dyes, which are used widely in the production of textiles, comprise a large group of organic molecules, the main characteristics of which are high stability in the aquatic environment and significant resistance to biodegradation under aerobic conditions. Azo dyes, along with intermediates and/or by-products, are not only harmful to aquatic life but are also potentially hazardous to human health by virtue of their carcinogenic and mutagenic properties. Moreover, these toxic compounds are difficult to remove using conventional wastewater treatments. In light of the above, we have chosen the azo dye Reactive Blue 198 (RB198) as a model compound for studies aimed at improving the efficiency of photoelectrochemical degradation processes.

For this purpose, we have fabricated a novel WO_3 electrode containing amorphous MoS_2 on a fluorine-doped tin oxide (FTO) glass substrate using straightforward and low-cost techniques involving a modified single-step sol-gel method for WO_3 and electrodeposition for MoS_2. The photoelectrocatalytic properties of the photocatalyst were evaluated by monitoring the efficiency of decolorization of RB198 under visible-light irradiation and low applied current density.

Experimental

Chemicals and solutions

Ammonium tungstate ($(NH_4)_{10}H_2(W_2O_7)_6$; 99.99% pure), ammonium tetrathiomolybdate ($(NH_4)_2MoS_4$; 99.97% pure), ethylene glycol (EG; 99.8% pure), and polyethylene glycol 300 (PEG 300) were purchased from Sigma-Aldrich, sodium sulfate (Na_2SO_4; 99.0% pure) was from J.T. Barker, potassium chloride (KCl; 98.5–105.0%, pure) was from Synth, and Reactive Blue 198 (RB198) was from Quimanil. All reagents were of analytical grade (unless otherwise stated) and were used without further purification. Aqueous solutions were prepared with water purified using a Millipore Milli-Q system (> 18.2 MΩ).

Preparation of FTO/WO_3, FTO/MoS_2, FTO/WO_3/MoS_2, and FTO/MoS_2/WO_3 electrodes

WO_3 nanostructures were synthesized using a modified sol-gel method developed by our research group [31]. The precursor salt $(NH_4)_{10}H_2(W_2O_7)_6$ was dissolved in a mixture of EG and PEG300 at a final concentration of 0.03 M and deposited over a total area of 1.0 cm^2 on FTO substrate. The thickness of a deposited layer is approximately 800 nm. In the preparation of FTO/MoS_2 and FTO/WO_3/MoS_2 electrodes, the electrodeposition of MoS_2 was performed according to a modified version of the method of Vrubel and Hu [32] using a solution containing 5 mM $(NH_4)_2MoS_4$ in 0.1 M KCl and an electrochemical cell with FTO or FTO/WO_3 as the working electrode, Pt as the counter electrode, and Ag/AgCl/KCl_{sat} as the reference electrode (Fig. 1a). Cyclic voltammetry was carried out in the potential range − 0.4 to 0.8 V at a scan rate of 50 mV s^{-1} with the number of cycles selected according to the level of deposition required. The FTO/MoS_2/WO_3 electrode was prepared by performing the two deposition steps in reverse order.

Characterization of electrodes

Morphological characterization of the electrodes was accomplished by field emission scanning electron microscopy (FE-SEM) using an Inspect F50 instrument (FEI-Thermo Fisher Scientific). An EDAX Genesis Apex energy dispersive X-ray spectrometer (EDS) was employed to perform microanalyses, while structural characterization was carried out by powder X-

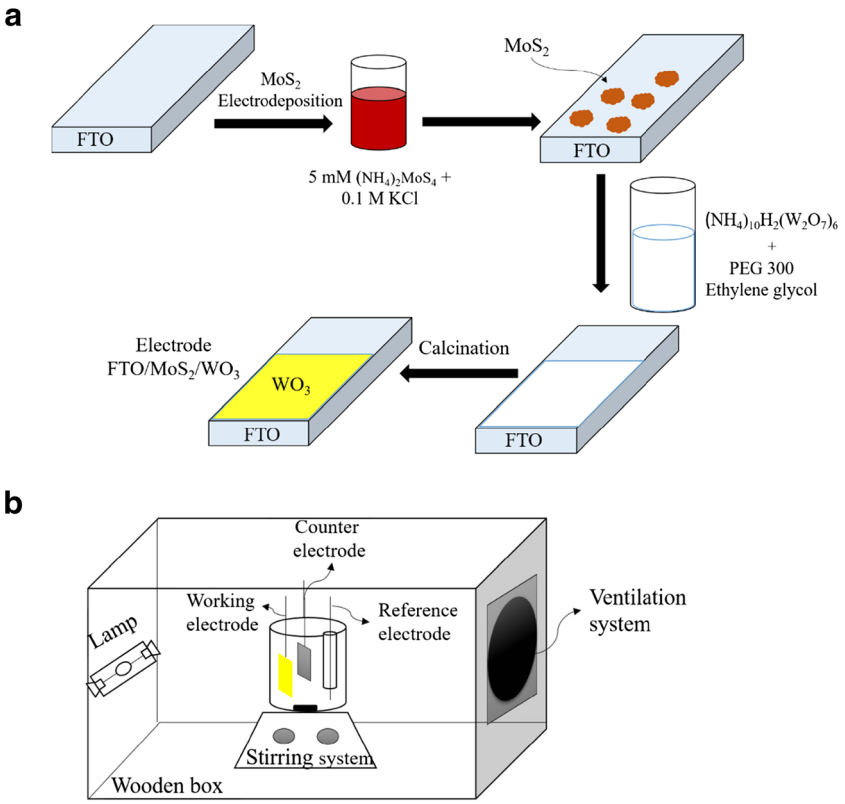

Fig. 1 **a** Method of preparation of $FTO/WO_3/MoS_2$ and $FTO/MoS_2/WO_3$ electrodes and (b) experimental set-up employed in the photoelectrochemical degradation of RB198 dye

ray diffraction (XRD) analysis using a Shimadzu model XRD-6000 diffractometer with Cu-Kα radiation and scanning in the 2θ range of 10 to 70°. UV diffuse reflectance spectra were recorded on a Varian Cary 5 UV–VIS spectrophotometer.

Photodegradation of Reactive Blue 198

The photoelectrocatalytic degradation of the dye RB198 was selected as a model system in order to evaluate the photocatalytic efficiency of the WO_3/MoS_2 electrodes, which were illuminated by back side. Experiments were conducted using a 70-mL electrochemical cell containing 10 ppm RB198 in 0.5 M Na_2SO_4 and housed in a laboratory-constructed system comprising a black wooden box fitted with an Osram HQI-TS 150 W metal halide lamp together with stirring and exhaust systems (Fig. 1b). The progress of the photoelectrochemical degradation of the dye was monitored spectrophotometrically.

Results and discussion

Characterization of MoS_2 films

Amorphous MoS_x can be electrodeposited onto FTO substrate from an aqueous solution of $(NH_4)_2MoS_4$ to form films of MoS_2 or MoS_3 depending on the applied potential. In the present study, cyclic voltammetry was employed in the electrodeposition process and the voltammetric plot of potential (in the range − 0.4 to 0.8 V) against current density (j) is shown in Fig. 2a. A film of MoS_3 is formed when cyclic voltammetry starts at anodic potential, but when electrodeposition ends at a cathodic potential with a reduction process, an MoS_2 film is produced [33]. Accordingly, two redox processes can be observed in the cyclic voltammogram, one relating to a peak of oxidation and another to reduction (labeled I and II, respectively, in Fig. 2a). The oxidation reaction can be represented by [32]:

$$Process\ \mathrm{I}: [MoS_4]^{2-} \rightarrow MoS_3 + {}^{1}/_{8}S_8 + 2e^- \quad (1)$$

Although the reduction of MoS_3 to form MoS_2 can occur, removal of MoS_3 is more likely due to the reverse reaction regenerating $[MoS_4]^{2-}$. The reductive deposition can then be attributed mainly to the following reaction:

$$Process\ \mathrm{II}: [MoS_4]^{2-} + 2H_2O + 2e^- \rightarrow MoS_2 + 2HS^- + 2OH^- \quad (2)$$

Hence, it is possible to produce an amorphous film of MoS_2 in admixture with MoS_3 through electrodeposition under the conditions applied.

Figure 2b presents an EDS point analysis of MoS_x electrodeposited after 20 cycles, a condition required to deposit sufficient material to quantify the elements. The spectrum verifies the presence of Mo and S, while quantification of the respective peaks revealed a Mo:S atom ratio of about 1:1.67, which is close to the stoichiometric value for MoS_2, thereby confirming that this is the major species in the film. The morphology of the MoS_2 film was investigated by FE-SEM analysis of the material electrodeposited after 20 cycles, a condition required to cover the substrate. The micrograph reproduced in Fig. 2c clearly shows the formation of amorphous particles with large grain sizes.

Characterization of WO_3/MoS_2 and MoS_2/WO_3 films

Examination of FE-SEM micrographs of a pure WO_3 film (Fig. 3a) revealed that the material had been successfully deposited over the entire substrate in a homogeneous and porous form with a mean pore diameter of 30 nm. FE-SEM micrographs of electrodes bearing WO_3 and MoS_2 deposited in combination were recorded after only two voltammetric cycles to ensure that the substrate was not completely covered. Figure 3b shows that the electrode with MoS_2 deposited on top of WO_3 comprised small WO_3 particles with some MoS_2 agglomerates on the surface of the film. In contrast, when WO_3 was deposited on top of MoS_2, particles of MoS_2 were not observed and the micrograph (Fig. 3c) showed only a continuous film with morphology similar to that obtained with pure WO_3.

An EDX analysis of the FTO/WO_3/MoS_2 electrode was performed with the aim of verifying the presence of the expected elements within the film. Although the spectrum (Online Resource 1) exhibited peaks that could be attributed to W, O, Mo, and S, it was not possible to carry out a quantitative analysis because the amount of electrodeposited MoS_2 was extremely small and could not be quantified with sufficient accuracy.

The phase structures of the electrodes were investigated by XRD analysis (Fig. 4). The diffractogram of the WO_3 film showed peaks at 23.3°, 23.7°, and 24.4° that are characteristic of a crystalline structure with a predominance of the monoclinic phase (JCPDS no. 43-1035). Additional diffraction peaks were observed that could be attributed to the FTO substrate (SnO_2, PDF no. 88-287). In contrast, the diffractogram of the MoS_2 film presented only FTO peaks, a result that was expected since the method employed deposited amorphous MoS_2 in the absence of heat treatment. Similarly, diffractograms of films of the combined materials, i.e., WO_3/MoS_2 and MoS_2/WO_3, exhibited no peaks that could be attributed to crystalline MoS_2.

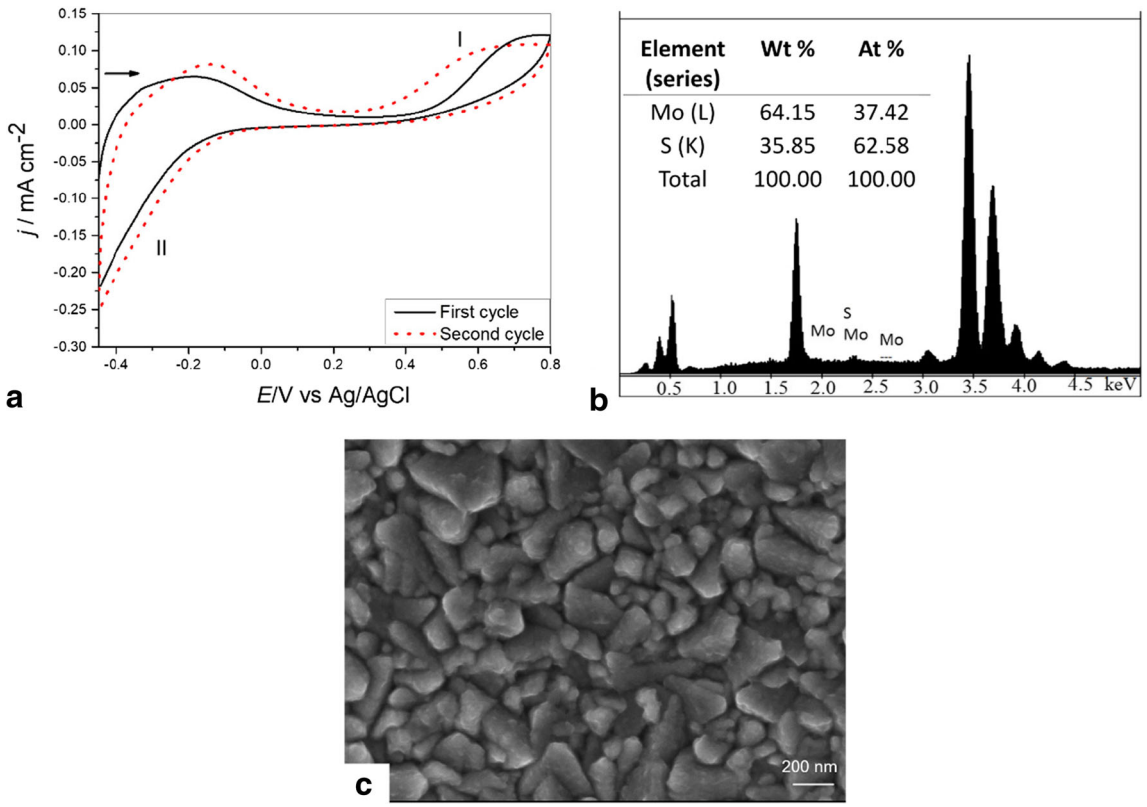

Fig. 2 **a** Cyclic voltammogram (recorded at a scan rate of 50 mV s^{-1}) of the deposition on FTO substrate of MoS_2 from an aqueous solution containing 5 mM $(NH_4)_2MoS_4$ and 0.1 M KCl, **b** EDS spectrum of a MoS_2 film, and **c** FE-SEM micrograph of a MoS_2 film

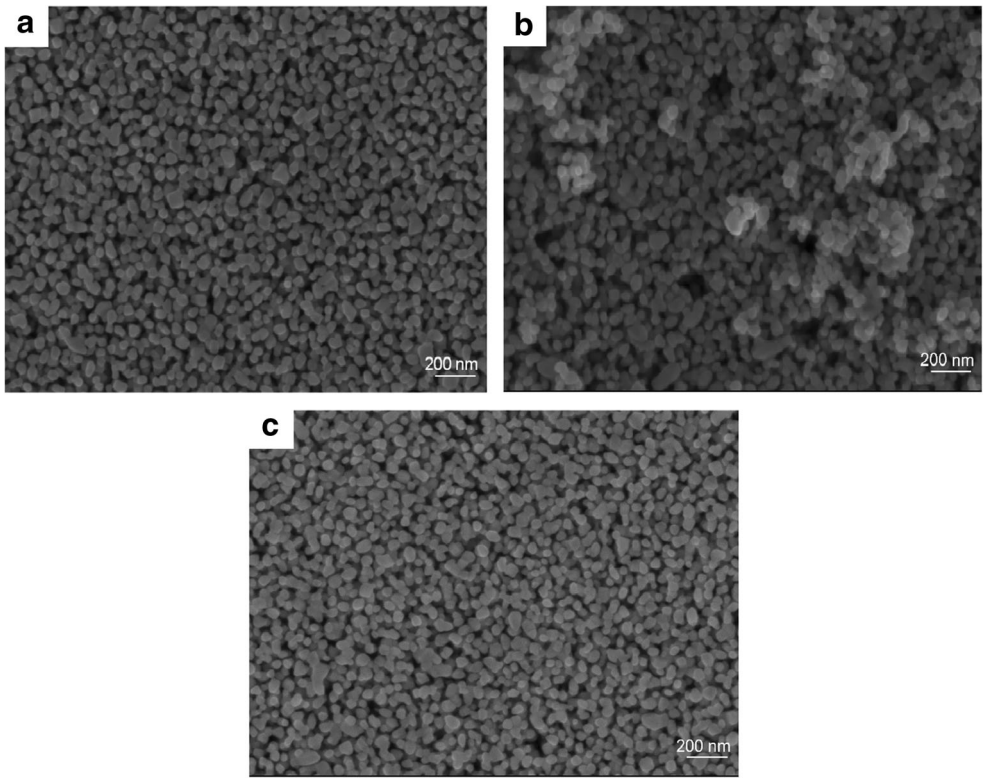

Fig. 3 FE-SEM micrographs of **a** FTO/WO_3, **b** FTO/WO_3/MoS_2, and **c** FTO/MoS_2/WO_3 electrodes

Band gap energies of FTO/WO_3, FTO/WO_3/MoS_2, and FTO/MoS_2/WO_3 electrodes were determined from UV–Vis diffuse reflectance spectra (Fig. 5a). All electrodes showed radiation absorption in the range of 300–450 nm corresponding to excitation of electrons of the valence band (VB) to the conduction band (CB) in WO_3. However, the intensity of the absorbance was slightly increased in the presence of MoS_2, and especially in WO_3/MoS_2. According to the Kubelka–Munk (KM) theory of reflectance, the KM function can be calculated from the equation: [34]

$$F(R) = \frac{(1-R)^2}{2R} \tag{3}$$

where R is reflectance. The $F(R)$ curves for FTO/WO_3, FTO/WO_3/MoS_2, and FTO/MoS_2/WO_3 electrodes are shown in Fig. 5b. The optical band gaps (E_g) of the WO_3 films were estimated by considering direct allowed transitions and were calculated from Tauc plots of $[F(R)h\nu]^2$ against photon energy ($E_{photon} = h\nu$). Values of E_g were established by extrapolating the linear portion of each plot to the x ($h\nu$) axis as shown in the Online Resource 2. No statistically significant differences were observed between the E_g values of the films produced (insert to Fig. 5a). Moreover, it was noted that MoS_2 promotes a slight shift towards the visible region according to Online Resource 2b.

From cyclic voltammetry studies, it is possibly observed that pure MoS_2 electrode did not present any photocurrent in 0.5 M Na_2SO_4 electrolyte according to Online Resource 3. However, the photocurrent was enhanced by a factor of up to 1.6 when MoS_2 is deposited on the WO_3 films.

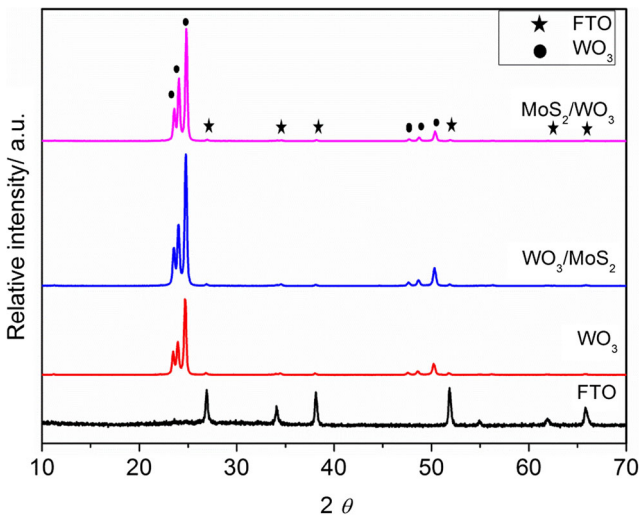

Fig. 4 XRD patterns of MoS_2, WO_3, WO_3/MoS_2, and MoS_2/WO_3 films deposited on FTO substrates

Evaluation of photodegradation efficiency of electrodes

The photocatalytic efficiencies of the electrodes were assessed by monitoring the decolorization of RB198 dye

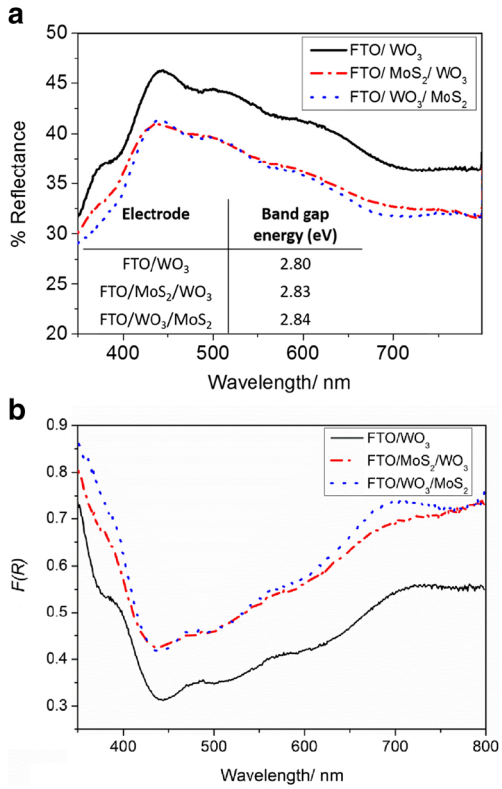

Fig. 5 **a** Diffuse reflectance spectra and **b** Kubelka–Munk absorption curves of FTO/WO_3, FTO/WO_3/MoS_2, and FTO/MoS_2/WO_3 electrodes

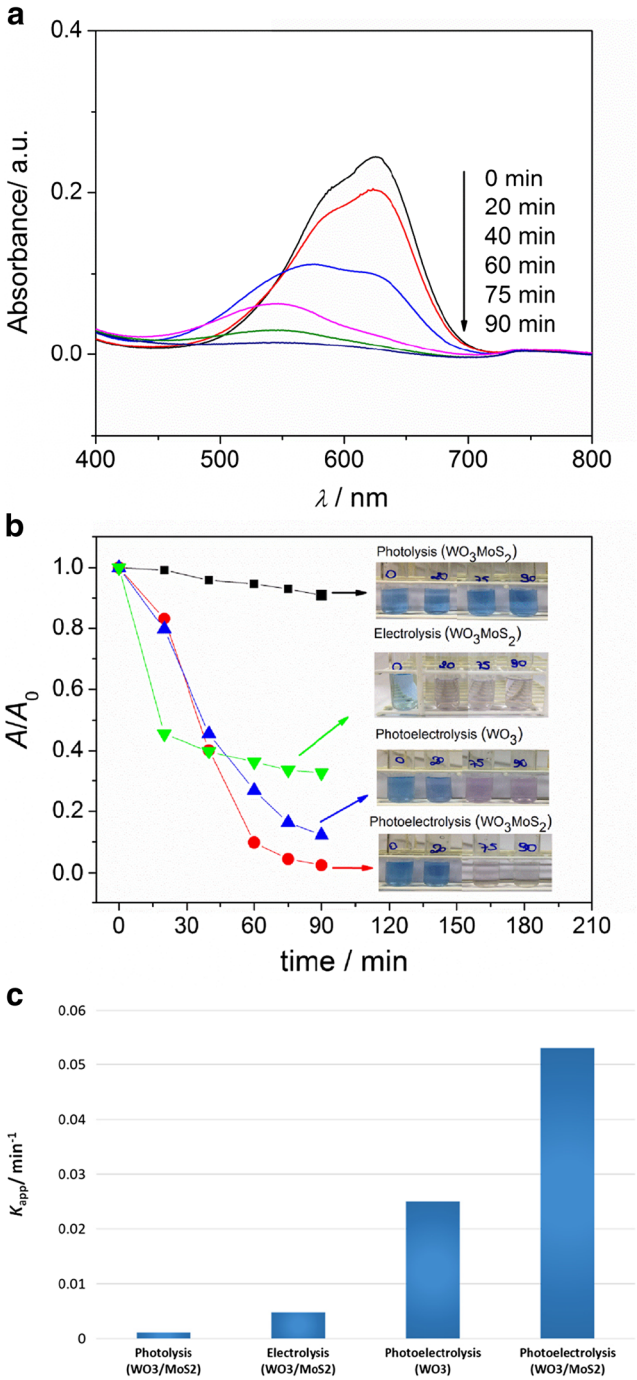

Fig. 6 **a** UV–Vis spectra of an aqueous solution containing 10 ppm RB198 in 0.5 M Na_2SO_4 as a function of time of photoelectrolysis using the FTO/WO_3/MoS_2 electrode with an applied current density of 5 mA cm^{-2}. Comparison of **b** the photodecolorization profiles of RB198 dye (measured at 625 nm) and **c** the apparent kinetic rate constants for photoelectrolysis, photolysis, and electrolysis processes with the FTO/WO_3/MoS_2 system and photoelectrolysis with the FTO/WO_3 electrode

during photoelectrochemical degradation. The absorbance spectra depicted in Fig. 6a were recorded during photoelectrolysis of the dye solution over 90 min of process time using the FTO/WO_3/MoS_2 electrode with an applied current density of 5 mA cm^{-2} (E_{cell} = 2.5 V). The chromophoric group of RB198 exhibits a broad band in the 625 nm region of the spectrum [35], and the intensity of this band gradually decreased as degradation of the dye progressed. It may also be noted that after 40 min of process, absorbance in the range 500–550 nm increases but from 60 min onwards, absorbance in the region decreases. This can be associated with the formation of intermediates or by-products during the process. For comparison purposes, the normalized 625-nm absorbance curves for photoelectrolysis, photolysis, and electrolysis processes using the FTO/WO_3/MoS_2 system, and for photoelectrolysis using the FTO/WO_3 electrode, are presented in Fig. 6b.

Using the FTO/WO_3/MoS_2 electrode, photoelectrolysis was more efficient than either photolysis or electrolysis, since hardly any dye decolorization was observed by photocatalytic action and the degree of decolorization was much reduced with electrolysis alone. Moreover, the performance of the FTO/WO_3/MoS_2 electrode was better than that of the FTO/WO_3 counterpart in the photoelectrochemical degradation of the dye. Complete decolorization of dye solution was attained after only 90 min of photoelectrolysis with the FTO/WO_3/MoS_2, and the current density applied during the process was lower than that generally reported in the literature for the degradation of dyes by electrolytic processes [36, 37]. Moreover, it is clear from the results shown in

Table 1 that the novel FTO/WO_3/MoS_2 electrode described in this work was particularly effective in decolorizing the textile dye in comparison with previously reported photoelectrolytic processes involving low current densities and commercial light sources. In the present study, 100% decolorization of the dye was achieved more rapidly than in other processes and did not require the addition of an oxidizing agent.

The decolorization profiles of the photoelectrochemical degradation of RB198 showed exponential decay in absorbance as a function of time for the entire process, indicating that the reaction was pseudo-first order. Apparent rate constants (k_{app}) could be calculated from the equation:

$$\ln\frac{A}{A_0} = -k_{app}t \tag{4}$$

where A_o and A are absorbance values measured at 0 and t min, respectively. Comparison of the apparent rate constants (Fig. 6c) for photoelectrolysis, photolysis, and electrolysis with the FTO/WO_3/MoS_2 electrode verified that the degradation rate in the photoelectrochemical reaction was increased significantly by synergism between the light-induced process and electrolysis. Moreover, photoelectrolysis with the FTO/WO_3/MoS_2 electrode presented a k_{app} value twofold higher than that obtained with the FTO/WO_3 electrode.

The higher photocatalytic activity presented by WO_3/MoS_2 compared with WO_3 can be explained on the basis of two possible mechanisms, namely (i) p–n heterojunction formation by band alignment in a crystalline material and (ii) activity of a cocatalyst. Both of these mechanisms would lead to a reduction in the e^-/h^+ recombination effect with the incidence of light resulting from the presence of MoS_2. Considering the first mechanism, in accordance with thermodynamic conditions, electrons injected into the CB of the p-type semiconductor would move to the CB of the n-type semiconductor and follow through to the substrate. On the other hand, the holes present in the VB would be displaced to the semiconductor/electrolyte interface where oxidation of an organic molecule could occur. In the second mechanism, in which a structured semiconductor gathers the light with a cocatalyst, the photocatalytic activity would be promoted or accelerated. Cocatalysts can act as reaction sites and catalyze processes, especially those related to O_2 and H_2 evolution, that promote charge separation and transport driven by interfaces formed between the cocatalyst and the semiconductor [22]. Additionally, in the presence of cocatalysts such as MoS_2 and CdS, electrons can react with O_2 to yield other oxygen species, including the superoxide radical anion [42].

Table 1 Comparison of the efficiencies of photoelectrochemical processes for the decolorization of dyes in aqueous solution

Electrode	Dye	Substrate concentration (ppm)	Cell volume (mL)	Area of electrode (cm^2)	Irradiation source	Applied current density (mA cm^{-2})	Time for total decolorization (min)	Reference
TiO_2[a]	Acid Orange 7	15	100	5.0	Radiometer (31.2 W m^{-2})	1.0	120	[38]
ZnO/Zn	Reactive Green 19	10	200	15.0	Philips lamp (7.7 W)	2.6	120	[39]
GF/TiO_2NTA[b]	Methyl Blue	5	80	4.0	Xenon lamp (35 W)	0.1	120 [c]	[40]
(EG)-ZnO[d]	Eosin Y (yellowish)	7 (0.1×10^{-4} M)	100	1.0	Quartz tungsten halogen lamp (300 W)	5.0	120	[41]
WO_3/MoS_2	Reactive Blue 198	10	70	1.0	Osram metal halide lamp (150 W)	5.0	90	Present study

[a] Generation of H_2O_2 on a gas diffusion electrode as counter electrode

[b] Graphene film decorated TiO_2 nano-tube array

[c] 65.9% decolorization of dye

[d] Exfoliated graphite–ZnO nanocomposite

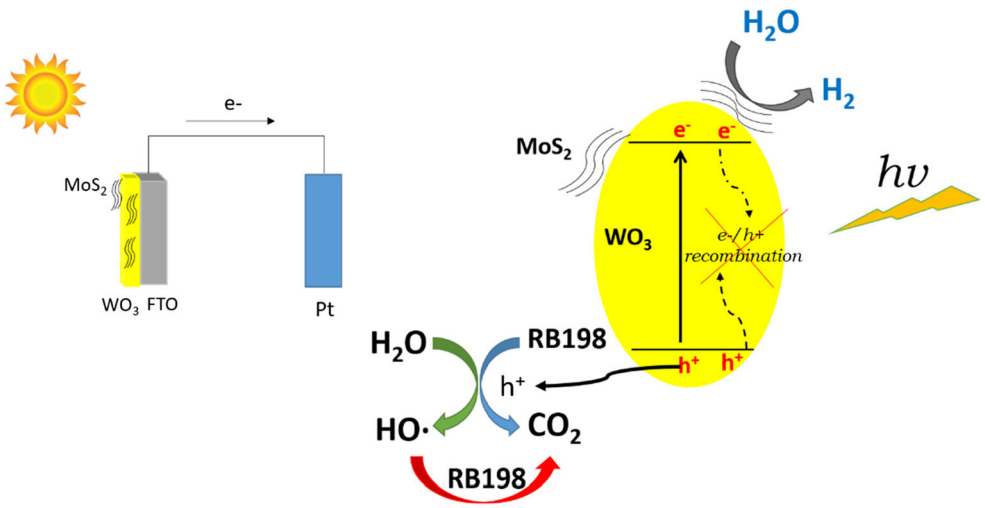

Fig. 7 Proposed mechanism of photoelectrochemical degradation of RB198 on the FTO/WO_3/MoS_2 electrode

A number of authors have investigated mechanisms that may be evoked when MoS_2 is used in combination with other materials. For example, Li et al. [9] synthesized a MoS_2/$BiVO_4$ composite and proposed that the presence of a well-defined staggered type II band alignment was responsible for heterostructure formation. However, it is unlikely that this type of mechanism prevails in the FTO/WO_3/MoS_2 electrode because the growth of MoS_2 on WO_3 film was amorphous and it did not exhibit a photocurrent. On the other hand, various studies have shown that MoS_2 can act as a cocatalyst. Thus, Zhao et al. [43] demonstrated that Cu_2O decorated with 1.0% (by weight) MoS_2 promoted a sevenfold increase in the photocurrent for H_2 production in comparison with Cu_2O alone. These authors suggested that the presence of MoS_2 increased the active sites of the composite and lessened the overpotential for the reduction of H^+ to H_2. Zhu et al. [44] studied photocatalytic H_2 evolution on a TiO_2–MoS_2 photocatalyst and verified that the photogenerated electrons in the CB of TiO_2 could be readily transferred to the MoS_2 cocatalyst, thereby promoting efficient charge separation and improving photocatalytic performance. These authors also showed that the oxidation of organic compounds could be carried out in the VB of TiO_2.

In light of the above, we consider that MoS_2 acts as catalyst for H_2 evolution in the FTO/WO_3/MoS_2 system and prevents e^-/h^+ recombination (Fig. 7). Moreover, MoS_2 accepts electrons from the CB of WO_3 and promotes the reduction of O_2 to the superoxide radical anion, an intermediate species that could react to form $\cdot OH^-$, thereby increasing the efficiency of photo-oxidation of organic compounds [30]. In this manner, charge transfer enhances the photo-oxidation of an adsorbed organic substrate by isolating electrons and holes in two distinct compartments. On this basis, the role of MoS_2 in the new semiconductor junction described herein must be that of cocatalyst.

Conclusions

This paper describes the successful synthesis of a new WO_3/MoS_2 photocatalyst on FTO substrate using simple and low-cost methods, namely modified sol-gel for WO_3 and electrodeposition for MoS_2. The developed electrode showed higher photocatalytic activity than its FTO/WO_3 counterpart and was more effective in the photoelectrochemical degradation of RB198, affording 100% decolorization of an aqueous solution of the dye in a relatively short time period at a low applied current density (5 mA cm^{-2}). Evidence presented herein supports the view that MoS_2 acts as a catalyst for H_2 evolution and prevents e^-/h^+ recombination in the WO_3 semiconductor. The novel approach of combining WO_3 and MoS_2 is promising and may prove to be very effective for the photocatalytic degradation of organic compounds and water splitting in the future.

Acknowledgements This work was supported by Fundação de Amparo à Pesquisa do Estado de São Paulo (FAPESP; grant no. 2014/10757-4 and 2015/00231-8), Centro de Pesquisa, Inovação e Difusão/FAPESP (CEPID/FAPESP; grant no. 2013/07296-2), Conselho Nacional de Desenvolvimento Científico e Tecnológico (CNPq), and Coordenação de Aperfeiçoamento de Pessoal de Nível Superior/Programa Professor Visitante do Exterior (CAPES/PVE).

References

1. Kudo A, Miseki Y (2009) Heterogeneous photocatalyst materials for water splitting. Chem Soc Rev 38:253–278
2. Chen HM, Chen CK, Liu R-S, Zhang L, Zhang J, Wilkinson DP (2012) Nano-architecture and material designs for water splitting photoelectrodes. Chem Soc Rev 41:5654–5671
3. Li Z, Liu J, Wang D, Gao Y, Shen J (2012) Cu_2O/Cu/TiO_2 nanotube ohmic heterojunction arrays with enhanced photocatalytic hydrogen production activity. Int J Hydrog Energy 37:6431–6437
4. Zhan F, Li J, Li W, Liu Y, Xie R, Yang Y, Li Y, Chen Q (2015) In situ formation of $CuWO_4$/WO_3 heterojunction plates array films

with enhanced photoelectrochemical properties. Int J Hydrog Energy 40:6512–6520
5. Wang HH, Zhang L, Chen Z, Hu J, Li S, Wang Z, Liu J, Wang X (2014a) Semiconductor heterojunction photocatalysts: design, construction, and photocatalytic performances. Chem Soc Rev 43: 5234–5244
6. Su J, Guo L, Bao N, Grimes CA (2011) Nanostructured WO_3/$BiVO_4$ heterojunction films for efficient photoelectrochemical water splitting. Nano Lett 11:1928–1933
7. Xia L, Bai J, Li J, Zeng Q, Li X, Zhou B (2016) A highly efficient $BiVO_4$/WO_3/W heterojunction photoanode for visible-light responsive dual photoelectrode photocatalytic fuel cell. Appl Catal B Environ 183:224–230
8. Gao H, Zhang P, Zhao J, Zhang Y, Hu J, Shao G (2017) Plasmon enhancement on photocatalytic hydrogen production over the Z-scheme photosynthetic heterojunction system. Appl Catal B Environ 210:297–305
9. Hu J, Wang L, Zhang P, Liang C (2016) Construction of solid-state Z-scheme carbon-modified TiO_2/WO_3 nano fibers with enhanced photocatalytic hydrogen production. J Power Sources 328:28–36
10. Zhang X, Zhang P, Wang L, Gao H, Zhao J, Liang C, Hu J, Shao G (2016a) Template-oriented synthesis of monodispersed SnS_2@ Sn_2 hetero-nanoflowers for Cr (VI) photoreduction. Appl Catal B Environ 192:17–25
11. Silva MR, Lucilha AC, Afonso R, Dall'Antonia LH, Andrade LV (2014) Photoelectrochemical properties of FTO/m-$BiVO_4$ electrode in different electrolytes solutions under visible light irradiation. Ionics (Kiel) 20:105–113
12. Li H, Yu K, Lei X, Guo B, Fu H, Zhu Z (2015a) Hydrothermal synthesis of novel MoS_2 /$BiVO_4$ hetero-nanoflowers with enhanced photocatalytic activity and a mechanism investigation. J Phys Chem C 119:22681–22689
13. Zhang J, Liu Z, Liu Z (2016b) Novel WO_3/Sb_2S_3 heterojunction photocatalyst based on WO_3 of different morphologies for enhanced efficiency in photoelectrochemical water splitting. ACS Appl Mater Interfaces 8:9684–9691
14. He H, Berglund SP, Xiao P, Chemelewski WD, Zhang Y, Mullins CB (2013) Nanostructured Bi_2S_3/WO_3 heterojunction films exhibiting enhanced photoelectrochemical performance. J Mater Chem A 1:12826–12834
15. Zhang M, Yang C, Pu W, Tan Y, Yang K, Zhang J (2014) Liquid phase deposition of WO_3/TiO_2 heterojunction films with high photoelectrocatalytic activity under visible light irradiation. Electrochim Acta 148:180–186
16. Wang D, Li R, Zhu J, Shi J, Han J, Zong X, Li C (2012) Photocatalytic water oxidation on $BiVO_4$ with the electrocatalyst as an oxidation cocatalyst: essential relations between electrocatalyst and photocatalyst. J Phys Chem C 116:5082–5089
17. Kim TW, Choi K-S (2014) Nanoporous BiVO4 photoanodes with dual-layer oxygen evolution catalysts for solar water splitting. Science 343:990–994
18. Asai R, Nemoto H, Jia Q, Saito K, Iwase A, Kudo A (2014) A visible light responsive rhodium and antimony-codoped $SrTiO_3$ powdered photocatalyst loaded with an IrO_2 cocatalyst for solar water splitting. Chem Commun (Camb) 50:2543–2546
19. Abe R, Shinmei K, Koumura N, Hara K, Ohtani B (2013) Visible-light-induced water splitting based on two-step photoexcitation between dye-sensitized layered niobate and tungsten oxide photocatalysts in the presence of a triiodide/iodide shuttle redox mediator. J Am Chem Soc 135:16872–16884
20. Wang C, Zhang X, Yuan B, Wang Y, Sun P, Wang D, Wei Y, Liu Y (2014b) Multi-heterojunction photocatalysts based on WO_3 nanorods: structural design and optimization for enhanced photocatalytic activity under visible light. Chem Eng J 237:29–37
21. Amaechi CI, Asogwa PU, Ekwealor ABC, Osuji RU, Maaza M, Ezema FI (2014) Fabrication and capacitive characteristics of conjugated polymer composite p-polyaniline/n-WO_3 heterojunction. Appl Phys A Mater Sci Process 117:1589–1598
22. Yang J, Wang D, Han H, Li C (2013) Roles of cocatalysts in photocatalysis and photoelectrocatalysis. Acc Chem Res 46: 1900–1909
23. Wang H, Lu Z, Sun J, Hymel TM, Cui Y (2014c) Electrochemical tuning of MoS_2 nanoparticles on three-dimensional substrate for efficient hydrogen. ACS Nano 8:4940–4947
24. Yu D, Feng Y, Zhu Y, Zhang X, Li B, Liu H (2011) Template synthesis and characterization of molybdenum disulfide nanotubules. Mater Res Bull 46:1504–1509
25. Xiang ZC, Zhang Z, Xu X, Zhang Q, Yuan C (2016) MoS_2 nanosheets array on carbon cloth as a 3D electrode for highly efficient electrochemical hydrogen evolution. Carbon N Y 98:84–89
26. Vrubel H, Merki D, Hu X (2012) Hydrogen evolution catalyzed by MoS_3 and MoS_2 particles. Energy Environ Sci 5:6136–6144
27. Zong X, Xing Z, Yu H, Bai Y, Max LGQ, Wang L (2014) Photocatalytic hydrogen production in a noble-metal-free system catalyzed by in situ grown molybdenum sulfide catalyst. J Catal 310:51–56
28. Du T, Wang N, Chen H, He H, Lin H, Liu K (2015) TiO_2-based solar cells sensitized by chemical-bath-deposited few-layer MoS_2. J Power Sources 275:943–949
29. Yuan YJ, Tu JR, Ye ZJ, Lu HW, Ji ZG, Hu B, Li Y-H, Cao D-P, Yu Z-T, Zou Z-G (2015) Visible-light-driven hydrogen production from water in a noble-metal-free system catalyzed by zinc porphyrin sensitized MoS_2/ZnO. Dyes Pigments 123:285–292
30. Tacchini I, Terrado E, Anson A, Martinez MT (2011) Preparation of a TiO_2-MoS_2 nanoparticle-based composite by solvothermal method with enhanced photoactivity for the degradation of organic molecules in water under UV light. Micro Nano Lett 6:932–936
31. Alves SA, Soares LL, Goulart LA, Mascaro LH (2016) Solvent effects on the photoelectrochemical properties of WO_3 and its application as dopamine sensor. J Solid State Electrochem:1–10
32. Vrubel H, Hu X (2013) Growth and activation of an amorphous molybdenum sulfide hydrogen evolving catalyst. ACS Catal 3: 2002–2011
33. Merki D, Hu X (2011) Recent developments of molybdenum and tungsten sulfides as hydrogen evolution catalysts. Energy Environ Sci 4:3878–3888
34. Adhikari S, Sarkar D, Maiti HS (2014) Synthesis and characterization of WO_3 spherical nanoparticles and nanorods. Mater Res Bull 49:325–330
35. Rajkumar K, Muthukumar M, Mangalaraja RV (2011) Electrocatalytic oxidation of reactive blue 198 using Sm^{3+} doped cerium oxide as a catalyst. Proc Int Conf Nanosci Eng Technol 14–18
36. Vasconcelos VM, Ribeiro FL, Migliorini FL, Alves SA, Steter JR, Baldan MR, Ferreira NG, Lanza MRV (2015) Electrochemical removal of Reactive Black 5 azo dye using non-commercial boron-doped diamond film anodes. Electrochim Acta 178:484–493
37. Migliorini FL, Braga NA, Alves SA, Lanza MRV, Baldan MR, Ferreira NG (2011) Anodic oxidation of wastewater containing the Reactive Orange 16 dye using heavily boron-doped diamond electrodes. J Hazard Mater 192:1683–1689
38. Garcia-segura S, Dosta S, Guilemany JM, Brillas E (2013) Solar photoelectrocatalytic degradation of Acid Orange 7 azo dye using a highly stable TiO_2 photoanode synthesized by atmospheric plasma spray. Appl Catal B Environ 132–133:142–150
39. Lee SL, Ho LN, Ong SA, Wong YS, Voon CH, Khalik WF, Yusoff NA, Nordin N (2015) Enhanced electricity generation and degradation of the azo dye Reactive Green 19 in a photocatalytic fuel cell using ZnO/Zn as the photoanode. J Clean Prod 127:579–584
40. Cheng X, Liu H, Chen Q, Li J, Wang P (2013) Preparation of graphene film decorated TiO_2 nano-tube array photoelectrode and

its enhanced visible light photocatalytic mechanism. Carbon N Y 66:450–458
41. Ntsendwana B, Sampath S, Mamba BB, Oluwafemi OS, Arotiba OA (2016) Photoelectrochemical degradation of eosin yellowish dye on exfoliated graphite–ZnO nanocomposite electrode. J Mater Sci Mater Electron 27:592–598
42. Li Q, Li X, Wageh S, Al-Ghamdi A A, Yu J (2015b) CdS/graphene nanocomposite photocatalysts. Adv Energy Mater
43. Zhao Y, Yang Z, Zhang Y, Lin J, Guo X, Ke Z, Hu P, Wang G, Yan Y-M, Sun K-N (2014) Cu2O decorated with co-catalyst MoS_2 for solar hydrogen production with enhanced efficiency under visible light. J Phys Chem C 118:14238–14245
44. Zhu Y, Ling Q, Liu Y, Wang H, Zhu Y (2015) Photocatalytic H_2 evolution on MoS_2-TiO_2 catalysts synthesized via mechanochemistry. Phys Chem Chem Phys 17:933–940